Fermi energies (E_F = −0.17 to −0.43 eV). We observe that the carrier density ($n_s \sim E_F^2$) changes linearly with V_g (Fig. 2C) and graphene has an intrinsic doping E_{F0} = −0.17 eV produced by charge transfer from the silica. Next, the analytic model is used to retrieve the protein permittivity from experimental results by adjusting a Lorentzian permittivity

$$\varepsilon_p(\omega) = n_1^2 = n_\infty^2 + \sum_{k=1}^{2} \frac{S_k^2}{\omega_k^2 - \omega^2 - i\omega\gamma_k} \quad (3)$$

Good agreement is observed between experimental and calculated spectra (Fig. 2B) for the protein Lorentzian parameters upon least-squares fitting. The extracted permittivity has a nondispersive term n_∞^2 = 2.08 and shows two absorption peaks at 1668 and 1532 cm^{-1}, matching the amide I and II bands, respectively (Fig. 2D). The fitted permittivity is also in good agreement with independent protein permittivity measurements from ellipsometry for n_∞^2 and IR reflection absorption spectroscopy (IRRAS) for S_k, ω_k, and γ_k (*20*). There is, however, a small discrepancy, which we attribute to a slight overestimate of plasmon-protein coupling in the theoretical model. These results indicate that the proposed graphene biosensor combines refractive index sensing, so far a prerogative of visible plasmonic sensors, with the unique chemical specificity of mid-IR spectroscopy, together with the extra degree of freedom enabled by the graphene electro-optical tunability.

The characteristics of our graphene biosensor become more evident by comparing its spectral response to that of a state-of-the-art metallic localized surface plasmon resonance (LSPR) sensor composed of a gold dipole-antenna array (Fig. 3). Both devices are first operated in a spectral range free of protein vibrational modes by setting graphene at V_g = −20 V and designing a gold dipole length L = 2.6 μm (Fig. 3A). Upon protein immobilization, we detect a resonance shift of 160 cm^{-1} for graphene, which is approximately 6 times the 27 cm^{-1} shift obtained with gold. Next, the operation spectrum is moved toward the protein amide I and II bands by setting graphene at V_g = −120 V and using a different gold sensor with L = 2.1 μm (Fig. 3B). Clearly, dynamic tunability of graphene is one of its main advantages over gold for surface-enhanced IR absorption (SEIRA), enabling sensing over a broad spectrum with a single device. In addition, for the SEIRA signal corresponding to the amide I band, the graphene sensor features a signal modulation of 27%, which is almost 3 times that observed with the gold sensor (11%).

The large spectral shifts and absorption signals confirm the unprecedented sensitivity of our graphene biosensor to the complex refractive index of the target molecule. For similar IR-frequency plasmons, the graphene atomic thickness leads to a higher confinement, resulting in a much larger spatial overlap between the mid-IR plasmonic field and the analyte. Figure 3C shows the near-field distribution of LSPR modes in graphene nanoribbons and gold dipole arrays calculated with a finite-element method. The field hotspots are located at the endpoints of the gold dipole and along the edges of the graphene nanoribbon. By computing the percentage of near-field intensity confined within a given distance d from the structure (Fig. 3D), we observe that 90% of the mode energy is confined within 15 nm from the graphene surface, whereas the same percentage is spread over a distance 500 nm away from the gold surface, thus confirming the tighter field confinement of graphene in the mid-IR. As the biosensing signal comes only from the field inside the target volume, we also calculate the field overlap with an 8-nm-thick protein bilayer, which is 29% for graphene versus only 4% for gold. The near-field intensity overlap can be experimentally extracted as the ratio of the relative resonance shift ($\Delta\omega/\omega$) and the permittivity variation ($\varepsilon_p - \varepsilon_{air}$) (*24*). This estimate yields 26% and 5% field overlap for graphene and gold, in good agreement with simulations (see above). These results demonstrate the ability of graphene to provide stronger light-protein interactions beyond state-of-the-art metallic plasmonic sensors; further improvement in the graphene quality should lead to even better sensitivity and spectral resolution.

REFERENCES AND NOTES

1. A. N. Grigorenko, M. Polini, K. S. Novoselov, *Nat. Photonics* **6**, 749–758 (2012).
2. F. J. García de Abajo, *Science* **339**, 917–918 (2013).
3. A. Vakil, N. Engheta, *Science* **332**, 1291–1294 (2011).
4. M. Jablan, H. Buljan, M. Soljacic, *Phys. Rev. B* **80**, 245435 (2009).
5. L. Ju *et al.*, *Nat. Nanotechnol.* **6**, 630–634 (2011).
6. H. Yan *et al.*, *Nat. Photonics* **7**, 394–399 (2013).
7. A. Woessner *et al.*, *Nat. Mater.* **14**, 421–425 (2015).
8. Z. Fang *et al.*, *ACS Nano* **7**, 2388–2395 (2013).
9. V. W. Brar *et al.*, *Nano Lett.* **13**, 2541–2547 (2013).
10. Z. Fei *et al.*, *Nature* **487**, 82–85 (2012).
11. F. H. L. Koppens *et al.*, *Nano Lett.* **11**, 3370–3377 (2011).
12. B. Vasić *et al. J. Appl. Phys.* **113**, 013110 (2013).
13. Y. Li *et al.*, *Nano Lett.* **14**, 1573–1577 (2014).
14. P. Li *et al.*, *Nano Lett.* **14**, 4400–4405 (2014).
15. P. R. Griffiths, J. A. De Haseth, *Fourier Transform Infrared Spectrometry* (Wiley, New York, 2007).
16. F. Neubrech *et al.*, *Phys. Rev. Lett.* **101**, 157403 (2008).
17. R. Adato, H. Altug, *Nat. Commun.* **4**, 2154 (2013).
18. C. Wu *et al.*, *Nat. Mater.* **11**, 69–75 (2012).
19. Y. Zhong *et al.*, *J. Nanophotonics* **9**, 093791 (2015).
20. See supplementary materials on *Science* Online.
21. R. Adato *et al.*, *Nano Lett.* **13**, 2584–2591 (2013).
22. F. J. García de Abajo, *ACS Photonics* **1**, 135–152 (2014).
23. E. D. Palik, *Handbook of Optical Constants of Solids* (Academic Press, New York, 1998).
24. J. D. Joannopoulos *et al.*, *Photonic Crystals: Molding the Flow of Light* (Princeton Univ. Press, Princeton, NJ, 2011).

ACKNOWLEDGMENTS

Supported by European Commission grants FP7-IEF-2013-625673-GRYPHON, Graphene Flagship CNECT-ICT-604391, and FP7-ICT-2013-613024-GRASP; the Spanish Ministry of Economy and Competitiveness (MINECO) "Fondo Europeo de Desarrollo Regional" (FEDER) through grant TEC2013-46168-R; NATO's Public Diplomacy Division in the framework of "Science for Peace"; European Union's Horizon 2020 research and innovation program under grant agreement No 644956; the Swiss National Science Foundation through project 133583; and Fundació Privada Cellex, the Severo Ochoa Program, and the Ramon y Cajal fellowship program. We also acknowledge École Polytechnique Fédérale de Lausanne and Center of MicroNano Technology for financial support and nanofabrication. This paper is dedicated to the memory of our friend and colleague, Julien Perruisseau-Carrier.

SUPPLEMENTARY MATERIALS

www.sciencemag.org/content/349/6244/165/suppl/DC1
Materials and Methods
Supplementary Text
Figs. S1 to S3
Reference (*25*, *26*)

11 April 2015; accepted 4 June 2015
10.1126/science.aab2051

GALAXY EVOLUTION

An over-massive black hole in a typical star-forming galaxy, 2 billion years after the Big Bang

Benny Trakhtenbrot,[1]* C. Megan Urry,[2,3,4] Francesca Civano,[3,5] David J. Rosario,[6] Martin Elvis,[5] Kevin Schawinski,[1] Hyewon Suh,[5,7] Angela Bongiorno,[8] Brooke D. Simmons[9]

Supermassive black holes (SMBHs) and their host galaxies are generally thought to coevolve, so that the SMBH achieves up to about 0.2 to 0.5% of the host galaxy mass in the present day. The radiation emitted from the growing SMBH is expected to affect star formation throughout the host galaxy. The relevance of this scenario at early cosmic epochs is not yet established. We present spectroscopic observations of a galaxy at redshift z = 3.328, which hosts an actively accreting, extremely massive BH, in its final stages of growth. The SMBH mass is roughly one-tenth the mass of the entire host galaxy, suggesting that it has grown much more efficiently than the host, contrary to models of synchronized coevolution. The host galaxy is forming stars at an intense rate, despite the presence of a SMBH-driven gas outflow.

Several lines of observational evidence, spanning a wide range of cosmic epochs, have led to a commonly accepted picture wherein supermassive black holes (SMBHs, $M_{BH} > 10^6\,M_\odot$; $M_\odot$ is the solar mass) coevolve with their host galaxies (*1*–*4*). Moreover, energy- and/or momentum-driven "feedback" from accreting SMBHs (Active Galactic Nuclei; AGN) is thought to quench star formation in the host galaxy (*5*). To directly test the relevance of such scenarios at

early cosmic epochs (high redshifts, z) requires the most basic properties of SMBHs and their hosts, including masses and growth rates, to be observed. Several observational studies found that at $z \leq 2$ (more than 3.3 billion years after the Big Bang), the typical BH-to-stellar mass ratio, M_{BH}/M_*, increases toward higher redshifts (*6*–*8*), suggesting that some SMBHs were able to gather mass more efficiently, or faster, than the stellar populations in their hosts. To date, measurements of M_{BH} at earlier epochs ($z > 2$) have only been conducted for small samples of extremely luminous objects [$L_{AGN} > 10^{46}$ erg s^{-1}; (*9*–*12*)] representing a rare subset of all accreting SMBHs, with number densities on the order of 1 to 10 per Gpc^3 [i.e., $\sim 10^{-9}$ to 10^{-8} Mpc^{-3}; (*13*)]. Moreover, the high AGN luminosities in such sources overwhelm the host galaxy emission and prohibit a reliable determination of M_*, and therefore of M_{BH}/M_*. We initiated an observational campaign aimed at estimating M_{BH} in x-ray–selected, unobscured $z \sim 3$ to 4 AGN within the Cosmic Evolution Survey field [COSMOS; (*14*)]. Such sources have lower AGN luminosities and are more abundant than the aforementioned luminous sources by factors of 100 to 1000 [e.g., (*13*, *15*)] and thus form a more representative subset of the general AGN population. Moreover, the fainter AGN luminosities and rich multiwavelength coverage of AGN within the COSMOS field enable reliable measurements of the mass and growth rate of the stellar populations in the host galaxies (M_* and star-formation rate, SFR).

CID–947 is an x-ray–selected, unobscured AGN at $z = 3.328$, detected in both *XMM-Newton* and *Chandra* x-ray imaging data of the COSMOS field [see fig. S4 and sections S2 and S4 in the supplementary materials (*16*)]. We obtained a near-infrared (IR) *K*-band spectrum of CID–947 using the MOSFIRE instrument at the W. M. Keck telescope, which at $z = 3.328$ covers the hydrogen Hβ broad emission line (see details in section S1 in the supplementary materials). The calibrated spectrum shows a very broad Hβ emission line, among other features (Fig. 1). Our spectral analysis indicates that the monochromatic AGN luminosity at rest-frame 5100 Å is $L_{5100} = 3.58^{+0.07}_{-0.08} \times 10^{45}$ ergs^{-1}. The typical line-of-sight velocity [i.e., the full-width at half-maximum of the line] is $11,330^{+800}_{-870}$ kms^{-1} (see section S1.2 in the supplementary materials). By combining this line width with the observed L_{5100} and relying on an empirically calibrated estimator for M_{BH}, based on the virial motion of ionized gas near the SMBH (*17*), we obtain $M_{BH} = 6.9^{+0.8}_{-1.2} \times 10^9 M_\odot$. All the reported measurement-related uncertainties are derived by a series of simulations and represent the 16th and 84th quantiles of the resulting distributions. These simulations indicate a SMBH mass larger than $3.6 \times 10^9 M_\odot$ at the 99% confidence level (see sections S1.2 and S3 in the supplementary materials for more details). Determinations of M_{BH} from single-epoch spectra of the Hβ emission line are known to also be affected by significant systematic uncertainties, of up to ~0.3 to 0.4 dex. For a detailed discussion of some of the systematics and related issues, see section S3 in the supplementary materials. This high M_{BH} is comparable with some of the most massive BHs known to date in the local universe (*18*) or with the masses of the biggest BHs in the much rarer, more luminous AGN at $z \sim 2$ to 4 [e.g., (*9*)]. The bolometric luminosity of CID–947 is in the range $L_{bol} \simeq (1.1 \text{ to } 2.2) \times 10^{46}$ erg s^{-1}, estimated either from the observed optical luminosity or the multiwavelength spectral energy distribution. Combined with the measured M_{BH}, we derive a normalized accretion rate of $L/L_{Edd} \simeq 0.01$ to 0.02. This value is lower, by at least an order of magnitude, than the accretion rates of known SMBHs at $z \sim 3.5$ [e.g., (*9*, *10*)]. Further assuming a standard radiative efficiency of 10%, we obtain an *e*-folding time scale for the SMBH mass of at least 2.1×10^9 years (Gy) (see section S3 in the supplementary materials), which is longer than the age of the universe at $z = 3.328$. By contrast, even the most extreme models for the emergence of "seed" BHs predict masses no larger than $M_{seed} \sim 10^6 M_\odot$ at $z \sim 10$ to 20 [e.g., (*19*)]. Therefore, the SMBH powering CID–947 had to grow at much higher accretion rates and at a high duty cycle in the past, to account for the high observed M_{BH} only 1.7 Gy after $z \simeq 20$. CID–947 could have evolved from a parent population similar to the fast-growing SMBHs observed in $z \gtrsim 5$ quasars, which have $L/L_{Edd} \sim 0.5$ to 1 and $M_{BH} \simeq 10^9 M_\odot$ [e.g., (*11*, *12*)]. The requirement for a high accretion rate in the very recent past is supported by the clear presence of a high-velocity outflow of ionized gas, observed in the rest-frame ultraviolet spectrum of the source (fig. S4). The broad absorption features of C IV λ1549 and Si IV λ1400 have maximal velocities of $v_{max} \simeq 12{,}000$ km s^{-1}. Assuming that this outflow is driven by radiation pressure, these velocities require accretion rates of $L/L_{Edd} \gtrsim 0.1$, as recently as 10^5 to 10^6 years before the observed epoch (see section S4 in the supplementary materials). We conclude that the SMBH powering CID–947 is in the final stages of growth and that we are witnessing the shut-down of accretion onto one of the most massive BHs known to date.

The rich collection of ancillary COSMOS multiwavelength data available for CID–947 enables us to study the basic properties of its host galaxy (see details in section S2 in the supplementary materials). A previously published analysis of the observed spectral energy distribution of the emission from the source reveals an appreciable stellar emission component, originating from $5.6^{+2.8}_{-0.4} \times 10^{10} M_\odot$ in stars (*20*). Our own analysis provides a yet lower stellar mass, of $M_* = 4.4^{+0.4}_{-0.5} \times 10^{10} M_\odot$. However, we focus on

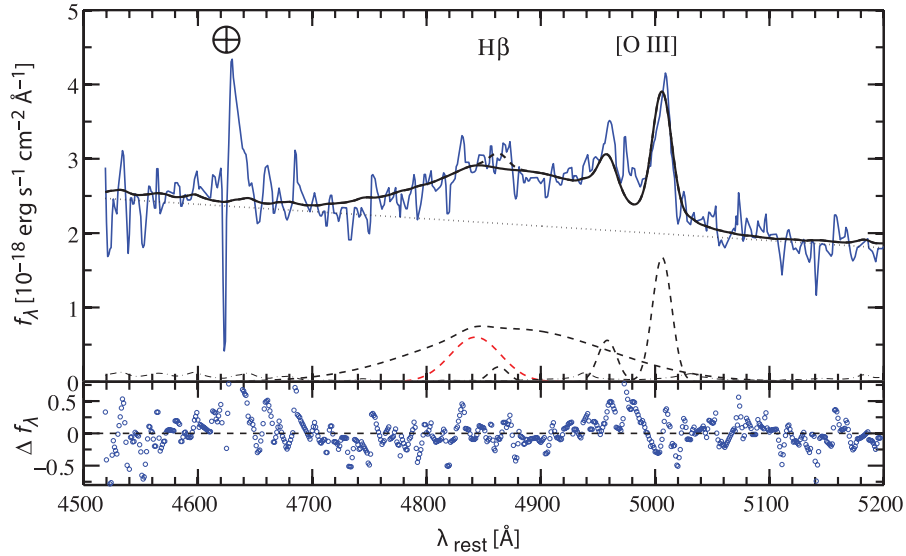

Fig. 1. The observed Keck/MOSFIRE spectrum and best-fit model for the Hβ emission complex of CID–947. The data are modeled with a linear continuum (dotted), a broadened iron template (dot-dashed), and a combination of broad and narrow Gaussians (dashed), which correspond to the Hβ and [O III] emission lines (see section S1.2 in the supplementary materials for details regarding the spectral modeling). The broad component of Hβ has a full width at half maximum of FWHM(Hβ) = 11330 km s^{-1}, which results in $M_{BH} = 6.9 \times 10^9 M_\odot$ and $M_{BH}/M_* = 1/8$. The red dashed line illustrates an alternative scenario, in which the SMBH mass derived from the Hβ line width would result in $M_{BH}/M_* = 1/100$ [i.e., FWHM(Hβ) = 3218 km s^{-1}], clearly at odds with the data. The spike at $\lambda_{rest} \simeq 4640$ Å is due to a sky feature. The bottom panel shows the residuals of the best-fit model.

[1]Department of Physics, Institute for Astronomy, ETH Zurich, Wolfgang-Pauli-Strasse 27, Zurich 8093, Switzerland. [2]Department of Physics, Yale University, Post Office Box 208120, New Haven, CT 06520-8120, USA. [3]Yale Center for Astronomy and Astrophysics, 260 Whitney Avenue, New Haven, CT 06520-8121, USA. [4]Department of Astronomy, Yale University, Post Office Box 208101, New Haven, CT 06520-8101, USA. [5]Harvard-Smithsonian Center for Astrophysics, 60 Garden Street, Cambridge, MA 02138, USA. [6]Max-Planck-Institut für Extraterrestrische Physik (MPE), Postfach 1312, 85741 Garching, Germany. [7]Institute for Astronomy, University of Hawaii, 2680 Woodlawn Drive, Honolulu, HI 96822, USA. [8]INAF-Osservatorio Astronomico di Roma, Via di Frascati 33, I-00040 Monteporzio Catone, Rome, Italy. [9]Oxford Astrophysics, Denys Wilkinson Building, Keble Road, Oxford OX1 3RH, UK.
***Corresponding author. E-mail: benny.trakhtenbrot@phys.ethz.ch**

the previously determined, higher stellar mass, as a conservative estimate. The source is also detected at far-IR and (sub)millimeter wavelengths, which allows us to constrain the SFR in the host galaxy to about 400 $M_\odot$ year^{-1}. The stellar mass of the host galaxy is consistent with the typical value for star-forming galaxies at $z \sim 3$ to 4 [i.e., the "break" in the mass function of galaxies; (*21*)]. Similarly, the combination of M_* and SFR is consistent with the typical values observed at $z \sim 3$ to 4, which appear to follow the so-called main sequence of star-forming galaxies (*22*). Thus, the host galaxy of CID–947 is a typical star-forming galaxy for its redshift, representing a population with a number density of about 5×10^{-5} Mpc^{-3} [e.g., (*21*)]. This suggests that neither the intense, ionizing radiation that emerged during the fast SMBH growth, nor the AGN-driven outflow, have quenched star formation in the host galaxy. The relatively high stellar mass and SFR of the host galaxy further suggest that it is unlikely that the AGN affected the host in yet earlier epochs. That is, even in this case of extreme SMBH growth, there is no sign of AGN-driven suppression of star formation in the host.

Our analysis indicates that the BH-to-stellar mass ratio for CID–947 is $M_{BH}/M_* \simeq 1/8$. In comparison, most local (dormant) high-mass BHs typically have $M_{BH}/M_* \sim 1/700$ to 1/500 [see Fig. 2 and, e.g., (*4*, *23*)]. The M_{BH}/M_* value that we find for CID–947 is thus far higher than typically observed in high-mass systems in the local universe, by at least an order of magnitude and more probably by a factor of about 50. The only local system with a comparably extreme mass ratio is the galaxy NGC 1277, which was reported to have $M_{BH}/M_* \simeq 1/7$ [with $M_{BH} = 1.7 \times 10^{10}\ M_\odot \simeq 2.5 \times M_{BH}$(CID–947); see (*24*), but also (*25*)]. At earlier epochs (still $z < 2$), the general trend is for M_{BH}/M_* to increase slightly with redshift, but typically not beyond $M_{BH}/M_* \sim 1/100$ (see Fig. 3). Only a few systems with reliable estimates of M_{BH} show M_{BH}/M_* reaching as high as 1/30 [e.g., (*6*–*8*)].

Given the high masses of both the SMBH and stellar population in CID–947, we expect this system to retain an extreme M_{BH}/M_* throughout its evolution, from $z = 3.328$ to the present-day universe. Because the M_{BH} that we find is already comparable to the most massive BHs known, it is unlikely that the SMBH will experience any further appreciable growth (i.e., beyond $M_{BH} \simeq 10^{10}\ M_\odot$). Indeed, if the SMBH accretes at the observed rate through $z = 2$, it will reach the extreme value of $\sim 10^{10}\ M_\odot$, and by $z = 1$ it will have a final mass of $\sim 2.5 \times 10^{10}\ M_\odot$. As for the host galaxy, we can constrain its subsequent growth following several different assumptions. First, if one simply assumes that the galaxy will become as massive as the most massive galaxies in the local universe [$M_* \simeq 10^{12}\ M_\odot$; (*26*)], then the implied final mass ratio is on the order of $M_{BH}/M_* \sim 1/100$. Alternatively, we consider more realistic scenarios for the future growth of the stellar population, relying on the observed mass (M_*) and growth rate (SFR). Our calculations involve different scenarios for the decay of star formation in the galaxy (see section S5 in the supplementary materials) and predict final stellar masses in the range $M_*(z = 0) \simeq (2 \text{ to } 7) \times 10^{11}\ M_\odot$, which is about an order of magnitude higher than the observed mass at $z = 3.328$. The

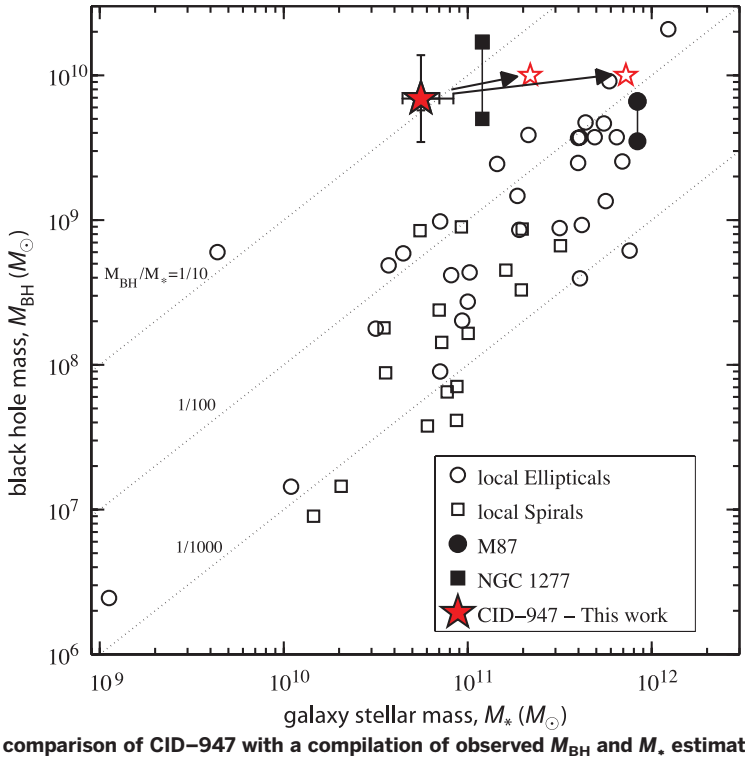

Fig. 2. A comparison of CID–947 with a compilation of observed M_{BH} and M_* estimates in the local universe [adapted from (*4*), assuming the tabulated bulge-to-total fractions]. CID–947 (red star) has a very high BH-to-stellar mass ratio of $M_{BH}/M_* \simeq 1/10$. The asymmetric error bars shown on M_{BH} and M_* represent measurement-related uncertainties, while the symmetric ones demonstrate systematic uncertainties of 0.3 dex (on M_{BH}) and 0.1 dex (on M_*). The masses inferred for subsequent growth scenarios are highlighted as empty red stars. The CID–947 system is expected to evolve only mildly in M_{BH} (perhaps to $\sim 10^{10}\ M_\odot$), but M_* should grow to at least $2 \times 10^{11}\ M_\odot$, and possibly to as much as $\sim 7 \times 10^{11}\ M_\odot$, by $z = 0$. The local galaxies NGC 1277 and M87, which could be considered as descendants of systems like CID–947, are highlighted as filled symbols [(*25*) and (*27*), respectively]. Some studies suggest these galaxies to have somewhat higher M_{BH}, and therefore relatively high mass ratios, of $M_{BH}/M_* = 1/7$ and 1/127, respectively (*24*, *28*).

Fig. 3. The observed cosmic evolution of the BH-to-stellar mass ratio, M_{BH}/M_*, and its extrapolation beyond $z \sim 2$. CID–947 (red star) has $M_{BH}/M_* = 1/8$ at $z \simeq 3.3$, which is higher by a factor of at least ~50 than the typical value in local, inactive galaxies (at most, $M_{BH}/M_* \sim 1/500$; dotted line). The error bars shown for CID–947 represent only the measurement-related uncertainties, propagating the uncertainties on M_{BH} and on M_*. The different data points at $z < 2$ represent typical (median) values for several samples with M_{BH}/M_* estimates, with uncertainties representing the scatter within each sample [filled symbols, open circles, and open triangles represent samples from (*7*), (*29*), and (*6*), respectively; adapted from (*7*)]. Even compared to the extrapolation of the evolutionary trend supported by these lower-redshift data, $M_{BH}/M_* \sim (z+1)^2$ [dashed line, scaled as in (*30*)], CID–947 has a significantly higher M_{BH}/M_*.

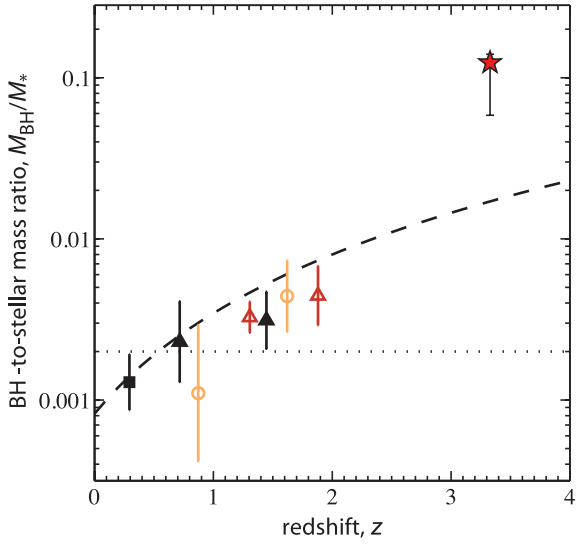

inferred final mass ratio is $M_{BH}/M_* \sim 1/50$. This growth can only occur if star formation continues for a relatively long period (≥1 Gy) and at a high rate (>50 $M_\odot$ year^{-1}). This would require the presence of a substantial reservoir, or the accretion, of cold gas, which, however, could not increase the SMBH mass by much. Finally, in the most extreme scenario, the star formation shuts down almost immediately (i.e., due to the AGN-driven outflow), and the system remains "frozen" at $M_{BH}/M_* \sim 1/10$ throughout cosmic time. If the SMBH does indeed grow further (i.e., beyond 10^{10} $M_\odot$), this would imply yet higher M_{BH}/M_*. Thus, the inferred final BH-to-stellar mass ratio for CID–947 is, in the most extreme scenarios, about $M_{BH}/M_* \sim 1/100$, and probably much higher (see Fig. 2).

CID–947 therefore represents a progenitor of the most extreme, high-mass systems in the local universe, like NGC 1277. Such systems are not detected in large numbers, perhaps due to observational selection biases. The above considerations indicate that the local relics of systems like CID–947 are galaxies with at least $M_* \sim 5 \times 10^{11}$ $M_\odot$. Such systems are predominantly quiescent (i.e., with low star-formation rates, SFR ≪ 1 $M_\odot$ year^{-1}) and relatively rare in the local universe, with typical number densities on the order of ~10^{-5} Mpc^{-3} (*26*). We conclude that CID–947 provides direct evidence that at least some of the most massive BHs, with $M_{BH} \gtrsim 10^{10}$ $M_\odot$, already in place just 2 Gy after the Big Bang, did not shut down star formation in their host galaxies. The host galaxies may experience appreciable mass growth in later epochs, without much further black hole growth, resulting in very high stellar masses but still relatively high M_{BH}/M_*. Lower-mass systems may follow markedly different coevolutionary paths. However, systems with M_{BH}/M_* as high as in CID–947 may be not as rare as previously thought, as they can be consistently observed among populations with number densities on the order of ~10^{-5} Mpc^{-3}, both at $z > 3$ and in the local universe, and not just among the rarest, most luminous quasars.

REFERENCES AND NOTES

1. L. Ferrarese, D. Merritt, *Astrophys. J.* **539**, L9–L12 (2000).
2. K. Gebhardt *et al.*, *Astrophys. J.* **539**, L13–L16 (2000).
3. X. Z. Zheng *et al.*, *Astrophys. J.* **707**, 1566–1577 (2009).
4. J. Kormendy, L. C. Ho, *Annu. Rev. Astron. Astrophys.* **51**, 511–653 (2013).
5. A. C. Fabian, *Annu. Rev. Astron. Astrophys.* **50**, 455–489 (2012).
6. A. Merloni *et al.*, *Astrophys. J.* **708**, 137–157 (2010).
7. R. Decarli *et al.*, *Mon. Not. R. Astron. Soc.* **402**, 2453–2461 (2010).
8. V. N. Bennert, M. W. Auger, T. Treu, J.-H. Woo, M. A. Malkan, *Astrophys. J.* **742**, 107 (2011).
9. O. Shemmer *et al.*, *Astrophys. J.* **614**, 547–557 (2004).
10. H. Netzer, P. Lira, B. Trakhtenbrot, O. Shemmer, I. Cury, *Astrophys. J.* **671**, 1256–1263 (2007).
11. G. De Rosa *et al.*, *Astrophys. J.* **739**, 56 (2011).
12. B. Trakhtenbrot, H. Netzer, P. Lira, O. Shemmer, *Astrophys. J.* **730**, 7 (2011).
13. D. Masters *et al.*, *Astrophys. J.* **755**, 169 (2012).
14. N. Z. Scoville *et al.*, *Astrophys. J. Suppl. Ser.* **172**, 1–8 (2007).
15. F. Civano *et al.*, *Astrophys. J.* **741**, 91 (2011).
16. Data and methods, supplementary text, figures and tables are available on *Science* Online.
17. Y. Shen, *Bull. Astron. Soc. Ind.* **41**, 61 (2013).
18. N. J. McConnell *et al.*, *Astrophys. J.* **756**, 179 (2012).
19. M. Volonteri, *Astron. Astrophys. Rev.* **18**, 279–315 (2010).
20. A. Bongiorno *et al.*, *Mon. Not. R. Astron. Soc.* **427**, 3103–3133 (2012).
21. O. Ilbert *et al.*, *Astron. Astrophys.* **556**, A55 (2013).
22. J. S. Speagle, C. L. Steinhardt, P. L. Capak, J. D. Silverman, *Astrophys. J. Suppl. Ser.* **214**, 15 (2014).
23. N. Häring, H. Rix, *Astrophys. J.* **604**, L89 (2004).
24. R. C. E. van den Bosch *et al.*, *Nature* **491**, 729–731 (2012).
25. E. Emsellem, *Mon. Not. R. Astron. Soc.* **433**, 1862–1870 (2013).
26. I. K. Baldry *et al.*, *Mon. Not. R. Astron. Soc.* **421**, 621 (2012).
27. J. L. Walsh, A. J. Barth, L. C. Ho, M. Sarzi, *Astrophys. J.* **770**, 86 (2013).
28. K. Gebhardt *et al.*, *Astrophys. J.* **729**, 119 (2011).
29. C. Y. Peng *et al.*, *Astrophys. J.* **649**, 616 (2006).
30. R. J. McLure, M. J. Jarvis, T. A. Targett, J. S. Dunlop, P. N. Best, *Mon. Not. R. Astron. Soc.* **368**, 1395–1403 (2006).

ACKNOWLEDGMENTS

The new MOSFIRE data presented herein were obtained at the W. M. Keck Observatory, which is operated as a scientific partnership among the California Institute of Technology, the University of California, and the National Aeronautics and Space Administration. The Observatory was made possible by the generous financial support of the W. M. Keck Foundation. We thank M. Kassis and the rest of the staff at the W. M. Keck observatories at Waimea, HI, for their support during the observing run. We recognize and acknowledge the very significant cultural role and reverence that the summit of Mauna Kea has always had within the indigenous Hawaiian community. We are most fortunate to have the opportunity to conduct observations from this mountain. Some of the analysis presented here is based on data products from observations made with European Southern Observatory (ESO) Telescopes at the La Silla Paranal Observatory under ESO program ID 179.A-2005 and on data products produced by TERAPIX and the Cambridge Astronomy Survey Unit on behalf of the UltraVISTA consortium. We are grateful to A. Faisst and M. Onodera for their assistance with the acquisition and reduction of the MOSFIRE data. We thank S. Tacchella, J. Woo, and W. Hartley for their assistance with some of the evolutionary calculations. K.S. gratefully acknowledges support from Swiss National Science Foundation Professorship grant PP00P2 138979/1. F.C. acknowledges financial support by the NASA grant GO3-14150C. M.E. acknowledges financial support by the NASA Chandra grant GO2-13127X. B.T. is a Zwicky Fellow at the ETH Zurich.

SUPPLEMENTARY MATERIALS

www.sciencemag.org/content/349/6244/168/suppl/DC1
Data, Methods, and Supplementary Text S1 to S4
Figs. S1 to S4
Table S1
References (*31*–*81*)

10 December 2014; accepted 29 May 2015
10.1126/science.aaa4506

ANIMAL PHYSIOLOGY

Exceptionally low daily energy expenditure in the bamboo-eating giant panda

Yonggang Nie,[1]* John R. Speakman,[2,3]* Qi Wu,[1]* Chenglin Zhang,[4] Yibo Hu,[1] Maohua Xia,[4] Li Yan,[1] Catherine Hambly,[3] Lu Wang,[2] Wei Wei,[1] Jinguo Zhang,[4] Fuwen Wei[1]†

The carnivoran giant panda has a specialized bamboo diet, to which its alimentary tract is poorly adapted. Measurements of daily energy expenditure across five captive and three wild pandas averaged 5.2 megajoules (MJ)/day, only 37.7% of the predicted value (13.8 MJ/day). For the wild pandas, the mean was 6.2 MJ/day, or 45% of the mammalian expectation. Pandas achieve this exceptionally low expenditure in part by reduced sizes of several vital organs and low physical activity. In addition, circulating levels of thyroid hormones thyroxine (T_4) and triiodothyronine (T_3) averaged 46.9 and 64%, respectively, of the levels expected for a eutherian mammal of comparable size. A giant panda–unique mutation in the *DUOX2* gene, critical for thyroid hormone synthesis, might explain these low thyroid hormone levels. A combination of morphological, behavioral, physiological, and genetic adaptations, leading to low energy expenditure, likely enables giant pandas to survive on a bamboo diet.

The giant panda (*Ailuropoda melanoleuca*) is an enigmatic, critically endangered bear endemic to China. Its diet is made up almost exclusively of bamboo, but it retains a short carnivoran alimentary tract and, consequently, has very low digestive efficiency (*1*–*3*). Therefore, the giant panda must feed for a large part of each day and consume large quantities of food relative to its body mass (*1*, *4*). This has led to speculation that giant pandas must also have low metabolic rates to achieve a daily energy balance (*1*). We report the first measurements of daily energy expenditure (DEE) of captive and free-living giant pandas, measured using the doubly labeled water (DLW) method (*5*) (see supplementary materials and methods). We validated these measurements using estimates of net energy assimilation and matched them with morphological, behavioral, physiological, and genetic data. We measured the DEE of five captive and three free-living pandas (supplementary text S1, tables S1.3 and S1.4). Across the captive individuals, the body mass averaged 91.1 kg and DEE averaged 4.6 ± 0.9 MJ/day (±SEM) (n = 5 animals). In the wild, the equivalent values were

[1]Key Laboratory of Animal Ecology and Conservation Biology, Institute of Zoology, Chinese Academy of Sciences, Beijing, China. [2]State Key Laboratory of Molecular Developmental Biology, Institute of Genetics and Developmental Biology, Chinese Academy of Sciences, Beijing, China. [3]Institute of Biological and Environmental Sciences, University of Aberdeen, Aberdeen, Scotland, UK. [4]Beijing Key Laboratory of Captive Wildlife Technologies, Beijing Zoo, Beijing, China.
*These authors contributed equally to this work.
†Corresponding author. E-mail: weifw@ioz.ac.cn

Science

An over-massive black hole in a typical star-forming galaxy, 2 billion years after the Big Bang

Benny Trakhtenbrot, C. Megan Urry, Francesca Civano, David J. Rosario, Martin Elvis, Kevin Schawinski, Hyewon Suh, Angela Bongiorno and Brooke D. Simmons

Science **349** (6244), 168-171.
DOI: 10.1126/science.aaa4506

Black hole out of kilter with theory

It is believed that black holes and their host galaxies coevolve, with the feedback from the black hole inducing star formation. Such a scenario requires certain timing and mass constraints for the black hole and the star-forming gas. Trakhtenbrot *et al.* looked at high-red shift galaxies, when the universe was only about 2 billion years old. They found a black hole that developed to maturity much earlier than would be expected and was about 10% of the total galactic mass ––much more than expected. Moreover, star formation continued after it would have been expected to stop.

Science, this issue p. 168